MAX-PLANCK-INSTITUT
FÜR QUANTENOPTIK

LMU LUDWIG-MAXIMILIANS-UNIVERSITÄT MÜNCHEN

Bachelor's Thesis

The Influence of Stark Shift in Multiphoton Ionization

Johannes Porsch

Faculty of Physics

Supervised by:
apl. Prof. Vladislav Yakovlev

July 22, 2025

MAX-PLANCK-INSTITUT
FÜR QUANTENOPTIK

LMU LUDWIG-MAXIMILIANS-UNIVERSITÄT MÜNCHEN

Bachelorarbeit

Der Einfluss des Stark-Effekts auf die Mehrphotonenionisation

Johannes Porsch

Fakultät für Physik

Supervisor:
apl. Prof. Vladislav Yakovlev

22. Juli 2025

Abstract

not ready...Multiphoton ionization of atoms in strong laser fields is a fundamental process in attosecond physics. In this work, we extend the strong-field approximation (SFA) by incorporating the influence of excited atomic states on ionization rates. Standard SFA formulations neglect these excited states, assuming that the laser field has no effect on the atom before ionization. However, in intense few-cycle laser pulses, the Stark shift and transient population of excited states can significantly modify ionization dynamics. We numerically solve the time-dependent Schrödinger equation (TDSE) using the tRecX code to extract time-dependent probability amplitudes for hydrogen's ground and excited states. These amplitudes are then integrated into the SFA formalism to evaluate their impact on ionization rates. The main findings are formula (2.19), the fact that stark shift plays a slightly bigger role in the ionization yield but both have very little contribution to the ionization dynamics. THe main cause for the improvement of the ionoizatin dynamics in contrast to previous SFA models is not stark effect, not ground state distortion and not transition to excited states. I.e something ODE does not capture but tRecX does.

Contents

List of Figures

1. Introduction

Ionization with an intense laser is one of the most fundamental processes in attosecond physics and quantum mechanics in general and has a broad range of applications, from high-harmonic generation to photoelectron spectroscopy and medical physics. Of particular interest is the 'response' of the electron to certain parts of the laser pulse at a given moment of time. From a classical point of view, the instantaneous ionization rate $\Gamma(t)$ provides a way to realize this concept. However, quantum mechanics presents a fundamental challenge: only probabilities can be measured, not the specific path an electron takes during ionization. In addition, predicting the *instantaneous* ionization of the electron at a given moment of time is difficult to reconcile with conventional quantum mechanics [**Ivanov2018**]. This is particularly due to the fact that the electron's response to the laser pulse is not instantaneous.

Significant research effort has been devoted to developing different ways of defining ionization rates [**agarwal2025generalapproximatorstrongfieldionization**, **Ivanov2018**]. The Strong Field Approximation (SFA) has become one of the standard theoretical frameworks for deriving ionization rates due to its simplicity and reasonably good agreement with numerical solutions of the time-dependent Schrödinger equation (TDSE). The way it reconciles with quantum mechanics is that within SFA, an expression exists that behaves just like an ionization rate, sharing characteristics of both classical and quantum mechanical physics. One very important property is that it matches the concept of an ionization rate under the assumption that the electron responds instantaneously to the electric field.

Two major problems exist with ionization rates within SFA. The first is their ambiguity, as the rate is not defined via a physically measurable quantity, making it gauge-dependent. The second is that the SFA itself is a crude approximation, significantly affecting the predicted ionization process in general. Further, in previous approaches, not only was the SFA applied, but additional approximations were made regarding the influence of the laser pulse on the atom, such as the Stark shift or transitions to excited states. This could explain why SFA can reconstruct overall ionization dynamics but fails to accurately reproduce off-cycle ionization dynamics.

Additionally, a significant discrepancy exists between the order of magnitude of ionization probabilities predicted by SFA and numerical solutions of the TDSE. This could have various causes, such as the SFA itself. However, it could also be due to the non-negligible impact of neglecting transitions to excited states.

The aim of this thesis is to investigate the influence of neglecting the laser pulse's impact on the atom in ionization dynamics. In particular, it examines whether the Stark effect or the distortion of the ground state has a greater influence on ionization dynamics. It also explores whether transitions to excited states could explain the large absolute difference between SFA-predicted ionization probabilities and numerical TDSE solutions. For this purpose, rigorous analytical expressions for the ionization rate within SFA are developed.

2. Theory

The structure of this Chapter largely follows [**Ivanov20012005**], with several modifications and adaptations to the context of this thesis.

The aim of this Chapter is to derive an expression for the instantaneous ionization rate (IIR) by analytically solving the time-dependent Schrödinger equation (TDSE) within the framework of the strong-field approximation (SFA).

2.1 Basic Formalism

The goal is to describe the time evolution of a quantum system under an external, time-dependent electromagnetic field in a form suitable for the strong-field approximation. To achieve this, a working formalism must be developed. The starting point is the time-dependent Schrödinger equation for a given Hamiltonian and the Maxwell equations, from which the light-matter interaction can be derived.

2.1.1 Schrödinger Equation

The time evolution of a quantum system $|\Psi(t)\rangle$ is determined by the time-dependent Schrödinger equation, a partial differential equation that describes the relationship between the change in time of $|\Psi(t)\rangle$ with a general Hamiltonian $\mathcal{H}(t)$:

$$i\hbar\frac{\partial}{\partial t}|\Psi(t)\rangle \overset{\text{a.u.}}{=} i\frac{\partial}{\partial t}|\Psi(t)\rangle = \hat{\mathcal{H}}(t)|\Psi(t)\rangle\,. \tag{2.1}$$

$\hat{\mathcal{H}}$ contains all relevant information for the time evolution, meaning it can be understood as being generated by the Hamiltonian. The formal solution of (2.1) depends on the time dependence of the Hamiltonian and the physical system under consideration. In the general case where the Hamiltonian does not commute with itself at different times, the solution

to (2.1) can be written as a Dyson series:

$$|\Psi(t)\rangle = \hat{\mathcal{U}}(t,t_0)\,|\Psi(t_0)\rangle = \hat{1}+\sum_{n=1}^{\infty}(-i)^n \int_{t_0}^{t} \mathrm{d}t_1 \int_{t_0}^{t_1} \mathrm{d}t_2 \cdots \int_{t_0}^{t_{n-1}} \mathrm{d}t_n \hat{\mathcal{H}}(t_n)\hat{\mathcal{H}}(t_{n-1})\cdots\hat{\mathcal{H}}(t_1)\,|\Psi(t_0)\rangle\,. \tag{2.2}$$

Physical setting This thesis focuses only on the ionization dynamics of a hydrogen atom exposed to an ultrashort and intense laser pulse. The Coulomb potential in atomic units is given by

$$\hat{\mathcal{H}}_{\mathrm{C}} \overset{\text{a.u.}}{=} \frac{1}{|\hat{\mathbf{r}}-\hat{\mathbf{r}}_0|}.$$

Since the TDSE is a *linear* partial differential equation, the Hamiltonian can be partitioned into separate parts. This partitioning can be performed in various ways, all of which are mathematically equivalent. For instance, a division into the unperturbed part and the interaction part yields:

$$\hat{\mathcal{H}}(t) \overset{\text{a.u.}}{=} \underbrace{\frac{\hat{\mathbf{P}}^2}{2}+\frac{1}{|\hat{\mathbf{r}}-\hat{\mathbf{r}}_0|}}_{\hat{\mathcal{H}}_0} + \hat{\mathcal{H}}_{\mathrm{I}}(t).$$

Solving the TDSE with $\hat{\mathcal{H}}_0$ provides the bound states of the hydrogen atom. The calculation can be found, for instance, in [**sakurai**] and will not be discussed here.

2.1.2 Light-Matter Interaction

A light wave consists of an electric field $\mathbf{E}(\underline{x},t)$ and a magnetic field $\mathbf{B}(\underline{x},t)$, which propagate through vacuum at the speed of light. These fields are defined by Maxwell's equations in empty space:

$$\begin{aligned} \nabla\cdot\mathbf{E} &= 0 \qquad & \nabla\times\mathbf{E} &= -\frac{\partial\mathbf{B}}{\partial t} \\ \nabla\cdot\mathbf{B} &= 0 \qquad & \nabla\times\mathbf{B} &= \mu_0\epsilon_0\frac{\partial\mathbf{E}}{\partial t} \end{aligned}$$

These equations can be solved using the potentials

$$\begin{aligned} \mathbf{E} &= -\nabla\varphi - \frac{\partial\mathbf{A}}{\partial t}, \\ \mathbf{B} &= \nabla\times\mathbf{A}, \end{aligned} \tag{2.3}$$

where $\mathbf{A}(\underline{x},t)$ is the vector potential and $\varphi(\underline{x},t)$ is the scalar potential. These potentials are not uniquely determined, as different choices can lead to the same physical fields. Specifically, the transformations

$$\mathbf{A} \to \mathbf{A}+\nabla\chi,\ \varphi \ \to \varphi - \frac{\partial\chi}{\partial t}, \tag{2.4}$$

with $\chi(\underline{x}, t)$ being an arbitrary smooth scalar function, also satisfy Maxwell's equations. This non-uniqueness is called gauge freedom and arises from the mathematical structure of Maxwell's equations. Selecting a particular gauge (i.e., fixing a certain χ) can be just a matter of convenience and simplify calculations.

2.1.3 Dipole Approximation

The dipole approximation is a widely used simplification in light-matter interaction. It applies when the wavelength of the optical field is significantly larger than both the size of the relevant bound electron states and the maximum displacement of a free electron. Additionally, it assumes that the magnetic field of the light has a negligible effect on the electron dynamics, requiring nonrelativistic particle velocities.

To derive this approximation, Maxwell's equations are first expressed in terms of the vector and scalar potentials, as defined in (2.3). This results in two coupled differential equations, which complicates the analysis. However, a simpler expression for the vector potential $\mathbf{A}$ can be obtained by selecting a specific gauge—the Lorentz gauge:

$$\partial_\mu \mathbf{A}^\mu = 0 \quad \text{or} \quad \nabla \cdot \mathbf{A} + \frac{\partial \varphi}{\partial t} = 0.$$

This gauge choice is achieved by solving the inhomogeneous wave equation for χ, which arises in the explicit calculation and is feasible when $\mathbf{A}$ and φ are known. With this gauge, Maxwell's equations decouple into:

$$\nabla^2 \varphi - \frac{\partial^2 \varphi}{\partial t^2} = 0,$$
$$\nabla^2 \mathbf{A} - \frac{\partial^2 \mathbf{A}}{\partial t^2} = 0.$$

The second equation is of particular interest, as it is a wave equation describing plane-wave solutions for $\mathbf{A}$:

$$\mathbf{A}(\underline{x}, t) = \mathbf{A}_0 \mathrm{e}^{\pm i(\mathbf{k}\cdot\mathbf{r} - \omega t)}.$$

Mathematically, the dipole approximation corresponds to the leading-order term in the Taylor expansion of $\mathrm{e}^{i\mathbf{k}\cdot\mathbf{r}}$. Consequently, the vector potential becomes spatially independent and can be approximated as [**bosmandipoleapprox**]:

$$\mathbf{A}(\underline{x}, t) = \mathbf{A}_0 \mathrm{e}^{\mp i\omega t} \exp\left\{\pm 2\pi i \frac{|\mathbf{r}|}{\lambda} \mathbf{e}_\mathbf{k} \cdot \mathbf{e}_\mathbf{r}\right\} \approx \mathbf{A}_0 \mathrm{e}^{\mp i\omega t} \left(1 + \mathcal{O}\left(\frac{|\mathbf{r}|}{\lambda}\right)\right) = \mathbf{A}(t)$$

This approximation holds as long as the wavelength λ is sufficiently large. Under these

conditions, the magnetic field simplifies to:

$$\mathbf{B} = \nabla \times \mathbf{A} \approx 0.$$

Although a different gauge may be chosen later, the physical description of the system remains unchanged. Of course the dipole approximation itself is gauge-independent, meaning that $\mathbf{B}$ remains approximately zero in any gauge. The Lorentz gauge is used here for convenience, as it provides an intuitive framework for the vector potential expansion.

The dipole approximation is valid for most experimental configurations, including the calculations in this work. However, it has limitations—for example, it breaks down in cases where strong-field ionization generates very fast electrons [**bosmandipoleapprox**, **breakdowndipoleapprox**].

This was the essence of the dipole approximation. To further simplify the description of the laser field in the Hamiltonian, the choice of gauge must be considered more carefully.

2.1.4 Length and Velocity Gauge

Calculating ionization rates in strong-field physics presents challenges due to the choice of gauge. While gauge transformations do not alter physical reality in classical electrodynamics, they can affect the practical computation of formulas derived in this Chapter, requiring careful consideration.

First, two basic expressions for the Hamiltonian in the velocity gauge and length gauge are derived using the dipole approximation. The semiclassical[1] Hamilton function for a free electron in an electric field is[2]:

$$\hat{\mathcal{H}}(\underline{x}, t) = \frac{1}{2m}(\hat{\mathbf{P}} + e\mathbf{A}(\underline{x}, t))^2 - e\varphi(\underline{x}, t) \tag{2.5}$$

Under the dipole approximation, this simplifies to:

$$\hat{\mathcal{H}}(\underline{x}, t) = \frac{\hat{\mathbf{P}}^2}{2m} + \frac{e}{m}\hat{\mathbf{P}} \cdot \mathbf{A}(t) + \frac{e^2}{2m}\mathbf{A}^2(t) - e\varphi(\underline{x}, t)$$

In most literature, φ is set to zero at this stage of the derivation because the sources of the electromagnetic wave lie outside the region of interest. While the dipole approximation does not strictly necessitate this assumption, φ will be left as is.

A common assumption in semiclassical Hamiltonians is that the vector potential alone drives electron state transitions, with no back-reaction from the electron [**bosmandipoleapprox**].

[1] In the semiclassical approach, quantum objects such as electrons are treated quantum-mechanically, while fields are treated classically.

[2] The derivation is provided in [**LandauLifschitzBand2**]. Note that for an electron, the charge is $-e$.

This approximation holds for sufficiently high laser intensities, though its validity may depend on specific conditions. The gauge transformation to the length gauge is performed via:

$$\chi = -\mathbf{A}(t) \cdot \mathbf{r} \tag{2.6}$$

with $\mathbf{r}(\underline{x}) = (x, y, z)$. This transformation sets $\mathbf{A}$ to zero, modifying φ as follows:

$$\nabla\varphi \to \nabla(\varphi + \mathbf{r} \cdot \frac{\partial \mathbf{A}}{\partial t}) = \nabla\varphi + \frac{\partial \mathbf{A}}{\partial t} = -\mathbf{E} \tag{2.7}$$

Integrating this equation from the origin to $\mathbf{r}$ yields the electric potential in the length gauge. With $\hat{\mathbf{r}}$ now quantized, the Hamiltonian becomes:

$$\hat{\mathcal{H}}(\underline{x}, t) = \frac{\hat{\mathbf{P}}^2}{2m} + e\hat{\mathbf{r}} \cdot \mathbf{E}$$

The time-dependent part $\hat{\mathcal{H}}(t)$ of the Hamiltonian can be expressed as:

$$\hat{\mathcal{H}}_{\mathrm{L}}(t) = -\hat{\mathbf{d}} \cdot \mathbf{E}(t) \tag{2.8}$$

where $\hat{\mathbf{d}} = -e\hat{\mathbf{r}}$ is the dipole operator and $\mathbf{E}(t)$ is the electric field.

An alternative gauge transformation, the velocity gauge, is also relevant. Using:

$$\chi = -\frac{e^2}{2m} \int_{-\infty}^{t} \mathbf{A}^2(t')\mathrm{d}t'$$

the dipole approximation leaves $\mathbf{A}$ unchanged but modifies φ as:

$$\varphi \to \varphi - \frac{e^2}{2m}\mathbf{A}^2(t)$$

resulting in the Hamiltonian:

$$\hat{\mathcal{H}}(\underline{x}, t) = \frac{\hat{\mathbf{P}}^2}{2m} + \frac{e}{m}\hat{\mathbf{P}} \cdot \mathbf{A}(t)$$

and

$$\hat{\mathcal{H}}_{\mathrm{V}}(t) = \frac{e}{m}\hat{\mathbf{P}} \cdot \mathbf{A}(t) \tag{2.9}$$

where φ is set to zero.

These are standard formulations of the interaction Hamiltonian for light-matter interactions. As with any gauge transformation, certain scenarios favor one gauge over another (see Chapter 4).

2.2 Strong Field Formalism

The difficulty with ionization arises from the existence of in some sense two Hilbert spaces: One for the bound states in the hydrogen atom that accounts for distortion of the wavefunction due to the laser field, and another for the continuum states that are primarily affected by the laser field but also influenced by the binding potential.

It will be shown that SFA provides a treatment for the second Hilbert space, simplifying its description. However, previous SFA formulations oversimplify the first Hilbert subspace to such an extent that there remains one Hilbert space for eigenstates unaffected by the laser field and another for continuum states unaffected by the binding potential.

SFA, in principle, concerns only the second part; neglecting the dynamics before ionization is not truly part of it. This section derives an expression that avoids excessive simplification of the first Hilbert space. Additionally, it will be demonstrated that there are two equivalent ways of solving the TDSE, which later diverge when approximations are introduced. Nevertheless, it becomes evident that these approaches nevertheless yield the same analytical result.

2.2.1 Projection into Subspaces

The full time-dependent Hamiltonian $\hat{\mathcal{H}}(t)$ is projected onto subspaces using projection operators defined by:

$$\hat{X} = \sum_n |\Psi_n\rangle \langle\Psi_n| \quad \text{and} \quad \hat{Y} = \hat{1} - \hat{X}$$

The use of projection operators for this type of problem is inspired by [**feshbachmethod**]. Projection operators are idempotent, i.e. $\hat{X}^2 = \hat{X}$. This property can be considered as the defining characteristic of projection operators, so applying them twice produces nothing new.

Here, $|\Psi_n\rangle$ represents the bound states of the atom. Using $\hat{X} + \hat{Y} = \hat{1}$, any partition of the Hamiltonian can be chosen. The most natural partitioning is first written as:

$$\hat{\mathcal{H}}(t) = \underbrace{\hat{X}\hat{\mathcal{H}}(t)\hat{X}}_{\hat{\mathcal{H}}_{\text{Bound}}(t)=\hat{\mathcal{H}}_0^{\text{Sub}}(t)} + \underbrace{\hat{Y}\hat{\mathcal{H}}(t)\hat{Y} + \hat{X}\hat{\mathcal{H}}(t)\hat{Y} + \hat{Y}\hat{\mathcal{H}}(t)\hat{X}}_{\hat{\mathcal{H}}_{\text{Cont}}(t)+\hat{\mathcal{H}}_{\text{Rec}}(t)+\hat{\mathcal{H}}_{\text{Ion}}(t)=\hat{\mathcal{H}}_{\text{I}}^{\text{Sub}}(t)} = \hat{\mathcal{H}}_0^{\text{Sub}}(t) + \hat{\mathcal{H}}_{\text{I}}^{\text{Sub}}(t)$$

The natural interpretation arises from the similarity to $\hat{\mathcal{H}}(t) = \hat{\mathcal{H}}_0(t) + \hat{\mathcal{H}}_{\text{I}}(t)$, where $\hat{\mathcal{H}}_{\text{I}}(t)$ represents the interacting perturbation (for instance, in the length gauge (2.8)), now applied to the full Hamiltonian projected onto subspaces. For reasons that will be explained later, this is referred to as the Subspace partition. While the notation may appear arbitrary now, its significance will become clear later.

The Hamiltonian can alternatively be partitioned into a different form, the full partition:

$$\hat{\mathcal{H}}(t) = \underbrace{\hat{X}\hat{\mathcal{H}}(t)\hat{X} + \hat{Y}\hat{\mathcal{H}}(t)\hat{Y} + \hat{X}\hat{\mathcal{H}}(t)\hat{Y}}_{\hat{\mathcal{H}}_{\mathrm{Bound}}(t)+\hat{\mathcal{H}}_{\mathrm{Cont}}(t)+\hat{\mathcal{H}}_{\mathrm{Rec}}(t)=\hat{\mathcal{H}}_0^{\mathrm{Full}}(t)} + \underbrace{\hat{Y}\hat{\mathcal{H}}(t)\hat{X}}_{\hat{\mathcal{H}}_{\mathrm{Ion}}(t)=\hat{\mathcal{H}}_{\mathrm{I}}^{\mathrm{Full}}(t)} = \hat{\mathcal{H}}_0^{\mathrm{Full}}(t) + \hat{\mathcal{H}}_{\mathrm{I}}^{\mathrm{Full}}(t)$$

The physical meaning of these terms can be interpreted as follows: In $\hat{\mathcal{H}}_{\mathrm{Bound}}(t)$, the electron remains within the subspace and can always be described by a superposition of bound states. Without ionization, this would be the only term governing the time evolution. In previous work, this part of the Hamiltonian was often simplified to the extent that the laser had no effect on the atom besides the ability to ionize it. Further details regarding physical effects, such as the Stark effect, can be found in Section 2.4.

$\hat{\mathcal{H}}_{\mathrm{Cont}}(t)$ describes similar dynamics, but in the subspace of continuum states rather than bound states. While in reality these two spaces cannot be completely separated, this distinction provides conceptual clarity. This is the part where the SFA will later be applied.

The remaining terms describe different physical processes. Two processes can occur: ionization of the electron or recombination with the atom. These processes are governed by the terms $\hat{\mathcal{H}}_{\mathrm{Rec}}(t)$ and $\hat{\mathcal{H}}_{\mathrm{Ion}}(t)$. In the present case, only one of these terms is relevant, and it will be shown later that $\hat{\mathcal{H}}_{\mathrm{Ion}}(t)$ is responsible for ionization, effectively "kicking" the electron out of the atom [**Ivanov20012005**].

While this approach may initially appear unnecessary, it establishes boundaries for the electron's behavior and provides useful intuition.

2.2.2 Dyson Equation

For determining the time evolution, care must be taken since the full Hamiltonian does not commute with itself at different times, requiring an exact treatment. As the full Dyson series (2.2) can be cumbersome to deal with, an alternative approach is used. This approach is enabled by the fact that the Hamiltonian can be split into two parts by projecting it into subspaces. The ansatz chosen here is with the Dyson equation. It relies on the time evolution operator and is completely equivalent to the TDSE and therefore to the Dyson series (2.2). It can be written in two forms that are equivalent in their raw formulation but may yield different results when approximations such as SFA are introduced.

The more intuitive form of the Dyson equation for this physical setting is given by:

$$\hat{\mathcal{U}}(t, t_0) = \hat{\mathcal{U}}_0^{\mathrm{Sub}}(t, t_0) - i\int_{t_0}^{t} \hat{\mathcal{U}}(t, t')\hat{\mathcal{H}}_{\mathrm{I}}^{\mathrm{Sub}}(t')\hat{\mathcal{U}}_0^{\mathrm{Sub}}(t', t_0)\mathrm{d}t' \tag{2.10}$$

Note that the "Sub" propagators are not identical to the "Full" propagators (2.11), but within the Dyson ansatz, the full propagator $\hat{\mathcal{U}}$ remains unchanged. This will change later

when SFA is introduced. Most formulas in this thesis can be best read from right to left, such as this one. The time evolution starts with the Hamiltonian projected onto the bound states. The interaction Hamiltonian then effectively ionizes the electron, inducing a transition to a virtual state, followed by propagation with the full time evolution. For more insights, refer to [**Ivanov20012005**].

The Dyson equation can also be expressed in a slightly different form:

$$\hat{\mathcal{U}}(t,t_0) = \hat{\mathcal{U}}_0^{\text{Full}}(t,t_0) - i\int_{t_0}^{t} \hat{\mathcal{U}}_0^{\text{Full}}(t,t')\hat{\mathcal{H}}_{\text{I}}^{\text{Full}}(t')\hat{\mathcal{U}}(t',t_0)\mathrm{d}t' \tag{2.11}$$

It can be verified that both equations satisfy the TDSE by direct substitution of $\hat{\mathcal{U}}(t,t_0)$. The main difference between the "Full" and "Sub" formulations is that the "initial" propagator on the right side is now the full time propagator instead of a reduced one. That motivates the acronym for both variants.

To simplify the analysis, the physical setting is further specified. Starting from the ground state of the atom, the time evolution is given by $\hat{\mathcal{U}}(t,t_0)\left|\Psi_0(t_0)\right\rangle$. For additional simplification, a projection onto a continuum state $\left|\mathbf{p}(t)\right\rangle$ at time t is considered. $\left|\mathbf{p}(t)\right\rangle$ does not represent a plane wave but rather an abstract state characterized by its momentum. Naturally, there is no overlap between $\left|\mathbf{p}(t)\right\rangle$ and $\hat{\mathcal{U}}_0^{\text{Sub}}(t,t_0)\left|\Psi_0(t_0)\right\rangle$ or with $\hat{\mathcal{U}}_0^{\text{Full}}(t,t_0)\left|\Psi_0(t_0)\right\rangle$, as the electron has not yet been ionized and no initial population in the continuum is assumed [**Ivanov20012005**]. Furthermore, when $\hat{\mathcal{H}}_{\text{I}}^{\text{Sub}}(t')$ and $\hat{\mathcal{H}}_{\text{I}}^{\text{Full}}(t')$ are expanded, and the orthogonality of bound states and continuum states is taken into account, most terms of $\hat{\mathcal{H}}_{\text{I}}(t')$ vanish. The remaining expressions are:

$$\left\langle \mathbf{p}(t)\right|\hat{\mathcal{U}}(t,t_0)\left|\Psi_0(t_0)\right\rangle\rangle = -i\int_{t_0}^{t}\left\langle \mathbf{p}(t)\right|\hat{\mathcal{U}}(t,t')\hat{Y}\hat{\mathcal{H}}(t')\hat{X}\hat{\mathcal{U}}_0^{\text{Sub}}(t',t_0)\left|\Psi_0(t_0)\right\rangle\mathrm{d}t' \tag{2.12}$$

and

$$\left\langle \mathbf{p}(t)\right|\hat{\mathcal{U}}(t,t_0)\left|\Psi_0(t_0)\right\rangle\rangle = -i\int_{t_0}^{t}\left\langle \mathbf{p}(t)\right|\hat{\mathcal{U}}_0^{\text{Full}}(t,t')\hat{Y}\hat{\mathcal{H}}(t')\hat{X}\hat{\mathcal{U}}(t',t_0)\left|\Psi_0(t_0)\right\rangle\mathrm{d}t' \tag{2.13}$$

Note: No approximations have been made; (2.12) and (2.13) are exact and equivalent to one another.

2.2.3 Strong Field Approximation

In principle, the strong field approximation involves neglecting the binding potential after ionization. This approximation is intuitively reasonable because the laser field becomes the dominant force acting on the electron, exerting significantly greater influence on the ionization dynamics than the Coulomb potential. It should be noted that SFA is not

restricted to high-intensity laser pulses; even for arbitrary small ionization probabilities, SFA implies that once ionization occurs, the laser pulse dominates the subsequent dynamics.

First, the "Sub" partitioning must be addressed. The time evolution operator after ionization can be expressed as:

$$\hat{\mathcal{U}}(t,t') \approx \hat{\mathcal{U}}_{\mathrm{SFA}}(t,t') = e^{-i\int_{t'}^{t}\hat{\mathcal{H}}_{\mathrm{SFA}}(t'')\mathrm{d}t''} \quad \text{and} \quad \hat{\mathcal{H}}_{\mathrm{SFA}}(t') = \hat{\mathcal{H}}(t) - \hat{\mathcal{H}}_{\mathrm{C}}$$

Similarly, for the "Full" partitioning:

$$\hat{\mathcal{U}}_0^{\mathrm{Full}}(t,t') \approx \hat{\mathcal{U}}_{\mathrm{SFA}}(t,t') = e^{-i\int_{t'}^{t}\hat{\mathcal{H}}_{\mathrm{SFA}}(t'')\mathrm{d}t''} \quad \text{and} \quad \hat{\mathcal{H}}_{\mathrm{SFA}}(t') = \hat{\mathcal{H}}(t) - \hat{\mathcal{H}}_{\mathrm{C}}$$

An exact expression for the SFA time evolution operator can be written, as it now commutes with itself at different times.

The SFA is particularly useful because the eigenstates of $\hat{H}_{\mathrm{SFA}}$ have an exact analytical solution. To see this, consider the semiclassical Hamiltonian in (2.5).

Classically, the physics driven by the momentum operator $\hat{\mathbf{P}}$ is known as the canonical momentum, given by:

$$\frac{\partial \mathcal{L}}{\partial \underline{\dot{x}}} = \mathbf{P} \overset{\mathrm{SI}}{=} m\dot{\mathbf{r}} - \frac{e}{c}\mathbf{A} \overset{\text{a.u.}}{=} \mathbf{p} - \mathbf{A} \tag{2.14}$$

where $\mathcal{L}$ is the Lagrangian of the system.

In this case, the canonical momentum is conserved. To verify this, setting $\varphi = 0$ (justified earlier) gives $\mathbf{E} = -\frac{\partial \mathbf{A}}{\partial t}$. The equation of motion for a charged particle in an electromagnetic field [**LandauLifschitzBand2**] is:

$$\frac{\mathrm{d}\mathbf{p}}{\mathrm{d}t} = -\mathbf{E} - (\dot{\mathbf{r}} \times \mathbf{B}) \approx \frac{\partial \mathbf{A}}{\partial t} = \frac{\mathrm{d}\mathbf{A}}{\mathrm{d}t}$$

Thus, $\frac{\mathrm{d}}{\mathrm{d}t}\mathbf{P} = 0$.

And also the energy of the system is clear:

$$E(t) = \dot{\mathbf{r}}\frac{\partial \mathcal{L}}{\partial \underline{\dot{x}}} - \mathcal{L} = \frac{(\mathbf{p}(t))^2}{2} \tag{2.15}$$

Note that the energy is not conserved, as the previous argument holds only for the canonical momentum, not the kinetic momentum.

The key observation is that $\langle \mathbf{p}(t)|$ is an eigenstate of $e^{-i\int_{t'}^{t}\hat{H}_{\mathrm{SFA}}(t'')\mathrm{d}t''}$. Combining (2.14) and (2.15) yields:

$$\langle \mathbf{p}(t)|\, e^{-i\int_{t'}^{t}\hat{\mathcal{H}}_{\mathrm{SFA}}(t'')\mathrm{d}t''} = \langle \mathbf{p}(t')|\, e^{-\frac{i}{2}\int_{t'}^{t}(\mathbf{P}+\mathbf{A}(t''))^2\mathrm{d}t''}$$

Here, $\mathbf{P}$ is time-independent, while $\mathbf{A}$ is not. Using the conservation of canonical mo-

mentum, the momentum at other times can be calculated. Of particular interest is the asymptotic limit when the laser field vanishes:

$$\mathbf{P} = \mathbf{p}(t'') + \mathbf{A}(t'') = \mathbf{p}(t \to \infty) + \mathbf{A}(t \to \infty) = \mathbf{p}$$

$\mathbf{p}$ is then simply the momentum of the electron after its 'recovery' from interaction with the laser field. $\langle \mathbf{p}(t')|$ can be rewritten using a similar argument:

$$\langle \mathbf{p}(t')| = \langle \mathbf{p} + \mathbf{A}(t')|$$

Combining these results leads to the following expressions for both "Sub" and "Full":

$$\langle \mathbf{p}(t)|\, \hat{\mathcal{U}}(t,t_0)\, |\Psi_0(t_0)\rangle\rangle = -i \int_{t_0}^{t} e^{-i\int_{t'}^{\infty}(\mathbf{p}+\mathbf{A}(t''))^2 \mathrm{d}t''} \langle \mathbf{p} + \mathbf{A}(t')|\, \hat{\mathcal{H}}(t')\hat{X}\, \hat{\mathcal{U}}_0^{\mathrm{Sub}}(t',t_0)\, |\Psi_0(t_0)\rangle\, \mathrm{d}t' \tag{2.16}$$

and

$$\langle \mathbf{p}(t)|\, \hat{\mathcal{U}}(t,t_0)\, |\Psi_0(t_0)\rangle\rangle = -i \int_{t_0}^{t} e^{-i\int_{t'}^{\infty}(\mathbf{p}+\mathbf{A}(t''))^2 \mathrm{d}t''} \langle \mathbf{p} + \mathbf{A}(t')|\, \hat{\mathcal{H}}(t')\hat{X}\, \hat{\mathcal{U}}(t',t_0)\, |\Psi_0(t_0)\rangle\, \mathrm{d}t' \tag{2.17}$$

Note that the SFA eliminates the difference in the left part of the integrand between "Sub" and "Full", making the two equations distinct. The final step introduces a new approximation for $\hat{\mathcal{U}}_0^{\mathrm{Sub}}(t',t_0)\, |\Psi_0(t_0)\rangle$ and $\hat{\mathcal{U}}(t',t_0)\, |\Psi_0(t_0)\rangle$.

Sub-Hilbertspace ansatz Regardless of the final form, the expression can be expanded in the bound states $|\Psi_n\rangle$. This is clear by considering the defining equation of the time evolution operator and observing that any overlap of $\hat{\mathcal{U}}_0^{\mathrm{Sub}}(t',t_0)\, |\Psi_0(t_0)\rangle$ with a state outside the bound-state representation would cancel out due to $\hat{X}$. With this consideration, an ansatz using the interaction picture can be formulated as[3]:

$$\hat{\mathcal{U}}_0^{\mathrm{Sub}}(t',t_0)\, |\Psi_0(t_0)\rangle = \sum_n c_n(t') e^{-iE_n t'}\, |\Psi_n\rangle$$

The factors $e^{-iE_n t'}$ are factored out to avoid potential numerical issues arising from their rapid oscillations.

In theory, this ansatz is exact but relies on the implicit assumption that the Hilbert spaces can be easily separated. Additionally, it assumes that the bound states remain unaffected by the laser field, which is not strictly true in reality. However, this approximation can be justified by the low laser intensity and the resulting ionization probability not

[3]Here, E_n represents the eigenenergies and not the electric field. If referring to the electric field, the notation would be a vector or a vector component.

exceeding 0.01.

Full Hilbertspace ansatz This case involves a more severe approximation. The primary advantage is that only the time evolution up to the ionization moment t' is required. The same assumptions regarding laser intensity and ionization probability apply here, justifying the approximation of the time evolution as a superposition of bound states:

$$\hat{\mathcal{U}}(t', t_0) \left|\Psi_0(t_0)\right\rangle = \sum_n c_n(t') e^{-iE_n t'} \left|\Psi_n\right\rangle$$

The key difference between the two ansatzes lies in the coefficients $c_n(t')$. In the subspace approach, the coefficients are obtained by solving the time-dependent Schrödinger equation for a wavefunction that is restricted to the subspace spanned by the bound states. This approach effectively cuts off ionization, forcing the electron to the subspace regardless of laser intensity. Implementing this leads to a system of ordinary differential equations for the coefficients, hence the name. In contrast, the other approach is fundamentally different. Here, the TDSE must be solved for a wavefunction in the full Hilbert space. In the atto/femtosecond regime, this demands substantial computational resources, as the electron exits the sub-Hilbert space during the process. For these numerical simulations, a solver called tRecX (discussed in Chapter 3) was employed.

Unlike other literature [**Theory_NPS**, **Ivanov20012005**], this ansatz does not neglect transitions between bound states prior to ionization. For example, the laser pulse may excite the electron without immediate ionization. The coefficients are expected to capture many of these interesting dynamics within the hydrogen atom before ionization occurs.

The final expression can now be presented. By simplifying the dipole transition matrix element $\mathbf{d}_n(\mathbf{p} + \mathbf{A}(t')) \overset{\text{a.u.}}{=} -\langle \mathbf{p} + \mathbf{A}(t')| \, \hat{\mathbf{r}} \, |\Psi_n\rangle$ between the bound state and the continuum state, the dipole approximation (2.8) can be applied, yielding:

$$\langle \mathbf{p}(t)|\Psi_n(t)\rangle = \frac{i}{2} \int_{t_0}^{t} e^{-i\int_{t'}^{\infty}(\mathbf{p}+A_z(t''))^2 \mathrm{d}t''} E_z(t') \sum_n c_n(t) e^{-iE_n t'} \langle \mathbf{p} + A_z(t')| \, \hat{d}_z \, |\Psi_n\rangle \, \mathrm{d}t' \quad (2.18)$$

Here, the electric field is polarized along the z-axis. This equation corresponds to the strong-field s-matrix in the length gauge, as found in many papers [**Theory_NPS**, **Ivanov20012005**], but with the difference that excited states and the influence of the laser field on the atom are not neglected.

2.3 Ionization Rates

The concept of an instantaneous ionization rate (IIR) is a powerful and intuitive tool for understanding the physics of strong-field ionization. It is frequently used to provide a time-resolved picture of the ionization process, for instance, by assigning a probability for an electron to be released at a specific moment during the laser pulse [**Ivanov2018**].

However, the concept of an ionization 'event' occurring at a precise instant in time is difficult to harmonize with quantum mechanics, such as Heisenberg's uncertainty principle. Strictly speaking, the only well-defined and directly measurable observable is the *total* ionization probability after the laser pulse has interacted with the atom. The IIR itself is not a direct quantum mechanical observable, and its definition can be challenging (gauge dependence).

This ambiguity leads to theoretical challenges, such as defining a working formalism for the tunneling delay time [**Ivanov2018**].

To address these challenges, alternative, unambiguous definitions have been proposed [**agarwal2025generalapproximatorstrongfieldionization**]. One such approach defines the IIR as a functional derivative of the total ionization probability with respect to the waveform of the ionizing laser pulse [**Ivanov2018**]. This method is inherently gauge-invariant because it is based on physically measurable quantities. While this thesis does not follow this particular formalism, it is important to acknowledge the subtleties involved in defining an ionization rate. The subsequent derivation proceeds within the SFA framework, which provides a tractable, but gauge-dependent expression for the IIR.

2.3.1 Derivation of Extended SFA Rate

The derivation mainly follows [**Theory_NPS**] with some modifications. First, the ionization probability is expressed as the amplitude of projection of the wavefunction onto the continuum subspace. The total ionization probability is obtained by integrating the ionization rate over the time domain. Therefore, the SFA rate (2.18) can be written as:

$$\begin{aligned}\lim_{t\to\infty} \langle\Psi(t)| \int \mathrm{d}^3p \, |p\rangle \langle p| \, \Psi(t)\rangle &= \int_{-\infty}^{\infty} \Gamma_{\mathrm{SFA}}(t)\mathrm{d}t \\ &= \int \mathrm{d}^3p \int_{-\infty}^{\infty}\int_{-\infty}^{\infty} \mathrm{d}t_1\mathrm{d}t_2 \, e^{\frac{i}{2}\int_{t_1}^{t_2}(\mathbf{p}+A_z(t''))^2\mathrm{d}t''} E_z(t_1)E_z(t_2) \\ &\quad \times \left(\sum_n e^{iE_nt_1} c_n^*(t_1) d_{z,n}^*(\mathbf{p}+A_z(t_1))\right)\left(\sum_n e^{-iE_nt_2} c_n(t_2) d_{z,n}(\mathbf{p}+A_z(t_2))\right)\end{aligned}$$

By changing variables to $t = \frac{t_2+t_1}{2}$ and $T = \frac{t_2-t_1}{2}$ and using the fact that the laser pulse is polarized along the z-axis, the expression becomes:

$$\begin{aligned}\Gamma_{\mathrm{SFA}}(t) = &\int \mathrm{d}^3p \int_{-\infty}^{\infty} \mathrm{d}T\, e^{\frac{i}{2}\int_{t-T}^{t+T}(\mathbf{p}+A_z(t''))^2\mathrm{d}t''} E_z(t-T)E_z(t+T) \\ &\times \left(\sum_n e^{i(t-T)E_n} c_n^*(t-T) d_{z,n}^*(\mathbf{p}+A_z(t-T))\right)\left(\sum_n e^{-i(t+T)E_n} c_n(t+T) d_{z,n}(\mathbf{p}+A_z(t+T))\right) \\ &= \sum_{n_1}\sum_{n_2}\int_0^{\infty}\mathrm{d}p\, p^2 \int_0^{\pi}\mathrm{d}\theta_p\, \sin\theta_p \int_0^{2\pi}\mathrm{d}\phi_p \int_{-\infty}^{\infty}\mathrm{d}T\, e^{\frac{i}{2}\int_{t-T}^{t+T}(\mathbf{p}+A_z(t''))^2\mathrm{d}t''} e^{i(t-T)E_{n_1}-i(t+T)E_{n_2}} \\ &\times E_z(t-T)E_z(t+T)c_{n_1}^*(t-T)c_{n_2}(t+T)d_{z,n_1}^*(\mathbf{p}+A_z(t-T))d_{z,n_2}(\mathbf{p}+A_z(t+T))\end{aligned}$$

The integration variable is changed from $\mathbf{p}$ to $\mathbf{p}+\mathbf{A}$, and with $\boldsymbol{\Delta}(t') = \mathbf{A}(t+t') - \mathbf{A}(t)$, the expression becomes:

$$\begin{aligned}&\sum_{n_1}\sum_{n_2}\int_0^{\infty}\mathrm{d}p\, p^2 \int_0^{\pi}\mathrm{d}\theta_p\, \sin\theta_p \int_0^{2\pi}\mathrm{d}\phi_p \int_{-\infty}^{\infty}\mathrm{d}T\, e^{\frac{i}{2}\int_{-T}^{T}(\mathbf{p}+\Delta_z(t''))^2\mathrm{d}t''} e^{i(t-T)E_{n_1}-i(t+T)E_{n_2}} \\ &\times E_z(t-T)E_z(t+T)c_{n_1}^*(t-T)c_{n_2}(t+T)d_{z,n_1}^*(\mathbf{p}+\Delta_z(-T))d_{z,n_2}(\mathbf{p}+\Delta_z(T))\end{aligned}$$

Also the integrand in the exponential function can be further simplified:

$$\begin{aligned}\frac{i}{2}\int_{-T}^{T}(\mathbf{p}+\Delta_z(t''))^2\mathrm{d}t'' &= i\mathbf{p}^2T + \frac{i}{2}\int_{-T}^{T}\Delta_z(t'')^2 + 2\mathbf{p}\cdot\Delta_z(t'')\mathrm{d}t'' \\ &= i\mathbf{p}^2T + ip\cos\theta_p\int_{-T}^{T}\Delta_z(t'')\mathrm{d}t'' + \frac{i}{2}\int_{-T}^{T}\Delta_z(t'')^2\mathrm{d}t''\end{aligned}$$

Following the notation used in the code as well as in [**Theory_NPS**], where

$$\bar{\boldsymbol{\Delta}}^k = \int_{-T}^{T}\boldsymbol{\Delta}^k(t')\mathrm{d}t' = \int_{-T}^{T}\left(\mathbf{A}(t+t')-\mathbf{A}(t)\right)^k\mathrm{d}t'$$

the final SFA rate to be implemented is given by:

$$\begin{aligned}\Gamma_{\mathrm{SFA}}(t) = &\sum_{n_1}\sum_{n_2}\int_0^{\infty}\mathrm{d}p\, p^2 \int_0^{\pi}\mathrm{d}\theta_p\, \sin\theta_p \int_0^{2\pi}\mathrm{d}\phi_p \int_{-\infty}^{\infty}\mathrm{d}T \\ &\times \exp\left(i\mathbf{p}^2T + ip\cos\theta_p\bar{\Delta}_z^k + \frac{i}{2}\bar{\Delta}_z^2 + i(t-T)E_{n_1} - i(t+T)E_{n_2}\right) \\ &\times E_z(t-T)E_z(t+T)c_{n_1}^*(t-T)c_{n_2}(t+T)d_{z,n_1}^*(\mathbf{p}+\Delta_z(-T))d_{z,n_2}(\mathbf{p}+\Delta_z(T))\end{aligned} \tag{2.19}$$

For numerical calculations, it can be convenient to split a complex integrand into its phase and absolute value. Although this is typically done with the given formula, the coefficients remain complex and may exhibit rapidly oscillating phase behavior.

2.4 Stark Shift

This section mainly follows [**subsycleacstarkshift**, **starkdelonekrainov**].

Phenomenology The Stark shift describes the shifting and splitting of energy levels due to the presence of an external electric field. This phenomenon arises from the interaction between the electric field and the atom's electric dipole moment. Two types of Stark shifts exist: the DC Stark shift and the AC Stark shift. DC stands for direct current, meaning the electric field is constant in time, while AC stands for alternating current, corresponding to a (rapidly) oscillating electric field. Under certain conditions (e.g., a laser pulse far off resonance), the AC Stark shift can be approximated as the quadratic DC Stark shift [**starkdelonekrainov**].

When the laser pulse is not far off resonance, significant changes to the energy levels of the bound states and to the electron dynamics can occur.

AC Stark Shift The electron wave function within the subspace of the bound states can be expressed as a superposition of bound states with coefficients $c_n(t)$:

$$|\Psi(t)\rangle = \sum_n c_n(t) e^{-iE_n t} |\Psi_n\rangle$$

where E_n are the eigenenergies and $c_n(t)$ are the complex coefficients. When considering electron dynamics before ionization, the coefficients can be interpreted as carrying two types of information. First, the amplitude of the coefficients represents the probability of finding the electron in a given state n. Second, the phase of the coefficients reflects changes in the energy level of state n. The second part can be interpreted as the subcycle AC Stark shift [**subsycleacstarkshift**]. This can be expressed mathematically as:

$$|\Psi(t)\rangle = \sum_n |c_n(t)| e^{-i\int_{-\infty}^{t} E_n + \delta E_n(t')\mathrm{d}t'} |\Psi_n\rangle \tag{2.20}$$

The dynamic stark energy shifts $\delta E_n(t')$ are of primary interest.

In the context of this thesis, the influence of the AC Stark shift on the ionization process is of particular interest. In previous derivations of the SFA rate, both the transition to excited states and the effect of the laser field on the ground state were neglected. However, with the extended version of the SFA rate (2.19), it becomes possible to account not only for the influence of the laser field on excited states but also to distinguish between the effects of the Stark shift and the depletion of the ground state (i.e., changes in the probability amplitude). While including many physical effects is theoretically appealing, it is not

always practical unless the impact of each approximation on the results is understood. The splitting of the coefficients into amplitude and phase allows this kind of distinction. The findings related to this question are presented in Chapter 4.

2.5 Strong Field Ionization

This section mostly follows [**manorammasterthesis**]. While not directly necessary for this thesis, these terms are frequently encountered in the literature and are briefly mentioned here for completeness. Ionization can occur in different ways, depending on the laser parameters and the atom or material used. To distinguish these processes, several parameters must be defined. According to [**Keldysh:1965ojf**], strong field ionization primarily depends on three parameters: the photon energy, the binding potential, and the ponderomotive energy.

Ponderomotive Energy The ponderomotive energy is defined as the cycle-averaged quiver energy of a free electron in an electromagnetic field [**manorammasterthesis**]. Since harmonic motion is experienced by the particle, the time-averaged kinetic energy is given by

$$\frac{1}{2}m\omega^2 \langle x^2 \rangle = \frac{e^2 E^2}{4m_e\omega^2} = \frac{E^2}{4\omega^2}$$

Keldysh Parameter The Keldysh parameter γ compares the ponderomotive energy with the ionization potential. It is defined as

$$\gamma = \sqrt{\frac{I_p}{2U_p}}$$

The ionization potential in the hydrogen atom is $I_p = 13.6\text{eV} = 0.5\text{au}$. Different regimes of ionization, each with distinct physical interpretations, can be defined based on the value of the Keldysh parameter.

2.5.1 Tunneling Ionization

This regime is typically characterized by $\gamma \ll 1$. Here, the laser pulse is sufficiently strong to distort the potential barrier. Alternatively, the tunneling regime can be defined as the regime where the quasi-static approximation holds, meaning the instantaneous ionization rate is entirely determined by the absolute value of the electric field at that time [**manorammasterthesis**]. This allows the ionization rate for DC and AC fields in this

regime to be calculated analytically [**tunnel_ion_complexatoms**].

$$\Gamma_{\mathrm{SFA}}(t) \propto \exp\left(-\frac{2}{3}\frac{(2I_p)^{3/2}}{F}\right)$$

Here, F represents the peak of the electric field for an AC field.

2.5.2 Multiphoton Ionization

The regime where $\gamma \gg 1$ is commonly referred to as multiphoton ionization. This occurs when the field strength is significantly weaker than in the tunneling regime. In other words, the multiphoton regime can be defined as the regime where

$$\Gamma_{\mathrm{SFA}}(t) \propto \mathbf{E}^{2N} \quad \text{with} \quad N = \frac{I_p}{E_e}$$

holds [**Ivanov20012005**]. This process can be visualized as the electron gaining energy while remaining under the barrier, effectively being heated up. Unlike the tunneling regime, this process is non-adiabatic. For further details, refer to [**Ivanov20012005**] and [**Keldysh:1965ojf**].

2.5.3 Intermediate Regime

This regime is particularly relevant for this thesis. The previous regimes describe limiting cases where the complementary process is negligible. However, in reality, a coexistence of both processes often occurs. In the intermediate regime, the tunneling process is no longer adiabatic. The potential barrier undergoes significant oscillations during the electron's tunneling time, allowing energy to be absorbed from the laser field while tunneling takes place.

3. Methods

This Chapter introduces the methods used throughout the thesis including numerical methods for solving or implementing certain types of equations, as well as physical methods used for result comparison or data interpretation.

To compare and verify the ionization rate from Chapter 2, the TDSE must be solved numerically without approximations. A reliable approach for comparison involves the use of the sampling method TIPTOE [**Park:18**], where the ionization yield from both are methods being compared. When expanding an existing model, it is particularly important to perform such comparisons to assess whether modifications align with expected outcomes.

3.1 Numerical Methods

To implement formula (2.18), the TDSE must be solved numerically in two different ways to obtain the coefficients $c_n(t)$. Two methods were used (numerical solver and ODE), each with its own advantages and disadvantages.

For numerically solving the TDSE without approximations, a solver called tRecX was used.

3.1.1 tRecX

tRecX is a C++ code designed for solving generalized inhomogeneous time-dependent Schrödinger-type equations in arbitrary dimensions and in a variety of coordinate systems [**Scrinzi_trecx**]. Ionization is typically challenging for numerical solvers because the electron leaves the subspace of bound states, making calculations computationally expensive. Additionally, the Coulomb potential decays only as $1/r$, raising the question of how to discretize the space and set boundary conditions.

tRecX employs various techniques that make it particularly suitable for light-atom interactions. For example, the method called "infinite-range exterior complex scaling" applies a unitary transformation to complex-scale space beyond a certain distance from the nucleus. This can be likened to the analytic continuation of a function into the complex plane. Fur-

thermore, the wavefunction is 'damped' by the complex-scaled region, preventing reflections at the boundary that could lead to numerical issues [**scrinzi_irecs**].

Moreover, tRecX allows the gauge (2.8), (2.9) in which the TDSE is solved to be specified, increasing its flexibility. This feature will be important later.

Throughout this thesis, tRecX was employed for two purposes.

First, it was used to solve the TDSE in the entire Hilbert space to obtain the coefficients $c_n(t)$, which are required for the improved SFA rate. For this purpose, the source code was modified to calculate the coefficients and store them in an appropriate format. Further details regarding the implementation can be found in Chapter 4.

Second, tRecX served as a reference within the TIPTOE experiment to evaluate the performance of the SFA rate with excited states (2.19).

3.1.2 System of ODEs

The coefficients of the wavefunction within the bound-state subspace were obtained using the interaction picture, and the resulting coupled system of differential equations was solved numerically. The calculation was implemented in Python, utilizing the ODE solver `solve_ivp` from SciPy's `integrate` module. The corresponding code is provided in the electronic appendix [**johannes_porsch_2025_16223179**] within the `HydrogenSolver` class. Further details on the implementation can be found in Chapter 4.

3.2 TIPTOE

This section mostly follows [**Park:18**] and [**manorammasterthesis**].

TIPTOE (Tunneling Ionization with a Perturbation for the Time-domain Observation of an Electric field) is a method for direct sampling of an electric pulse in the femtosecond to attosecond regime using quasistatic subcycle tunneling ionization in a gaseous medium or air.

A typical TIPTOE simulation consists of two linearly polarized laser pulses: a "fundamental" and a "signal" pulse, similar to common pump-probe experiments. The drive pulse is the pulse to be sampled, with the ionization yield of a certain medium providing the measurement. In first order, the ionization rate can be approximated as

$$\Gamma(E_\mathrm{F} + E_\mathrm{S}) \approx \Gamma(E_\mathrm{F}) + E_\mathrm{S} \frac{\mathrm{d}\Gamma(E_\mathrm{S})}{\mathrm{d}E}\bigg|_{E=E_\mathrm{F}} \tag{3.1}$$

In this approximation, depletion of the ground state is neglected. The total ionization yield

N_{total} obtained by the two pulses is given by

$$N_{\text{total}} = N_{\text{F}} + \delta N = \int \mathrm{d}t\, \Gamma(E_{\text{F}}(t)) + \int \mathrm{d}t\, E_{\text{S}}(t)\, \frac{\mathrm{d}\Gamma(E_{\text{S}}(t))}{\mathrm{d}E}\bigg|_{E=E_{\text{F}}(t)}$$

By varying the delay τ between the two pulses, the ionization yield takes on different values. From this, it follows that:

$$\delta N(\tau) \propto E_{\text{S}}(\tau) \tag{3.2}$$

Thus, the field amplitude of the signal pulse can be sampled by measuring the ionization yield for different delays. The TIPTOE method can be applied across a broad spectral range of the signal pulse, as long as the fundamental pulse is shorter than 1.5 optical cycles.

This method provides a way to compare ionization dynamics predicted by a numerical solver and by the SFA rate (2.19). TIPTOE is particularly useful because numerical simulations can provide good predictions about ionization probabilities, while analytical models describe ionization rates. A TIPTOE simulation can help reconstruct the ionization dynamics, which is especially relevant in the context of this thesis. Later, the ionization rate $\Gamma(E_{\text{F}} + E_{\text{S}})$ will be integrated over the full time domain, and the ionization yield for different delays will be compared with the results from the numerical solution of the TDSE. The results are shown in Chapter 5.

For better visualization of the underlying physics in TIPTOE, the background ionization N_{F} from $E_{\text{F}}(t)$ is subtracted, and the ionization yield is normalized, so the formula in plot 5.1 reads

$$\frac{N_{\text{total}} - N_{\text{F}}}{N_{\text{max}}} = \frac{\delta N(\tau)}{N_{\text{max}}} \tag{3.3}$$

However, interesting physics can also be observed by comparing only the total ionization yield, as discussed later in Chapter 5.

Typically, TIPTOE is not used for this kind of analysis but rather for its sampling capabilities. Instantaneous ionization rates are highly useful because TIPTOE enables sampling of the electric field of a laser pulse in the femtosecond to attosecond regime, which has broad applications in fields such as laser spectroscopy and medical physics.

3.3 GASFIR

GASFIR stands for General Approximator for Strong Field Ionization Rates. It is an analytical retrieval tool designed to reconstruct data obtained from numerical solutions of the TDSE. The model was validated for hydrogen and shows good agreement with existing theories in the quasi-static limit of tunneling ionization, not only for hydrogen but also for helium and neon [**agarwal2025generalapproximatorstrongfieldionization**].

The working principle of GASFIR is based on the use of ionization probabilities to retrieve ionization rates. The approach employs the idea from SFA that the rates can be expressed as $\int \mathrm{d}T K(t,T)$, where $K(t,T)$ is a kernel function. Later in the code, the kernel function is also visible, with the modifications applied there.

GASFIR is not part of this thesis; however, this thesis was partially motivated by the idea that an improvement of the SFA formalism could benefit the GASFIR approach.

4. Implementation

This Chapter describes the implementation of the formula (2.19) and the associated challenges. The majority of the code was originally developed by the authors of [**Theory_NPS**]. Modifications made to both the tRecX source code and the SFA rate are documented in the electronic appendix [**johannes_porsch_2025_16223179**]. The two main new components in this implementation are the coefficients $c_n(t)$ and the dipole matrix elements $d_{z,n}(\mathbf{p})$, while the remaining parts were straightforward.

4.1 Coefficients

As mentioned in Chapter 2, the Dyson equation can be written in two ways, resulting in two different expressions for the strong field s-matrix. The difference between the two approaches lies only in the coefficients.

4.1.1 Subspace Ansatz

To understand how the coefficients are determined, the defining equation can be examined:

$$\hat{\mathcal{U}}_0^{\mathrm{Sub}}(t',t_0)\,|\Psi_0(t_0)\rangle = \sum_n c_n(t') e^{-iE_n t'}\,|\Psi_n\rangle$$

with

$$i\frac{\partial}{\partial t'}\hat{\mathcal{U}}_0^{\mathrm{Sub}}(t',t_0) = \hat{X}\hat{\mathcal{H}}(t')\hat{X}\,\hat{\mathcal{U}}_0^{\mathrm{Sub}}(t',t_0) \tag{4.1}$$

This can be interpreted as the wavefunction being restricted to the subspace. The derivation for the coefficients is outlined below.

First, $\hat{\mathcal{H}}(t)$ is split into two parts: $\hat{\mathcal{H}}_0$ and $\hat{\mathcal{H}}_{\mathrm{I}}(t)$, where the eigenstates of $\hat{\mathcal{H}}_0$ are $|\Psi_n\rangle$ and the eigenenergies are E_n. By substituting the ansatz above into (4.1) and multiplying with $\langle\Psi_m|$, the coefficients $c_n(t)$ are obtained:

$$i\dot{c}_m(t) = \sum_n c_n(t) e^{-i\omega_{nm}t}\,\langle\Psi_m|\hat{\mathcal{H}}_{\mathrm{I}}(t)|\Psi_n\rangle$$

with $\omega_{nm} = E_n - E_m$.

Several challenges arise when implementing this approach. First, while $\sum_n$ theoretically extends from zero to infinity, numerical simulations require a finite number of states. The justification for the chosen number of states must be considered, along with ensuring that truncating the sum does not introduce numerical instabilities.

Additionally, increasing the number of coefficients affects previously calculated values. For example, solving only for the ground state $c_0(t)$ results in $|c_0(t)|^2 = 1$. However, the ground-state occupation decreases as more states are included in the sum, illustrating the *coupled* nature of the system of ODEs.

As the number of states increases, the results (e.g., the rates) should converge. However, since the electron is constrained to the subspace, including highly excited states may introduce numerical instabilities. For intensities around $10^{14}\frac{\mathrm{W}}{\mathrm{cm}^2}$ and longer wavelengths ($800\mathrm{nm} - 1200\mathrm{nm}$), allowing occupation of higher states led to unphysical oscillations in the rates. Under typical conditions, the electron would ionize, but since ionization is suppressed in this approach, excitation to high-energy states can cause the model to fail. Thus, a balance must be made between accuracy and numerical stability. In the simulations presented later, a maximum of $n = 3$ was used for the bound state calculations.[1] This choice is justified by analyzing the population dynamics of the hydrogen atom over time, where most pre-ionization dynamics are governed by the first few bound states—particularly $1s$, $2s$, $2p$, and $3p$—meaning that including additional states has minimal impact on the lower-state coefficients.

Note: This discussion pertains not to the number of bound states included in the final simulations, but rather to the number considered when solving the ODE. While only the ground state could have been used in the SFA rate calculations, the influence of higher bound states on the ground state must still be assessed. This justification is provided here.

Further, equation (4.1.1) is gauge dependent because of $\langle m|\hat{\mathcal{H}}_{\mathrm{I}}(t)|n\rangle$. Either the length gauge (2.8) or the velocity gauge (2.9) can be chosen. Which gauge should be used to obtain the most meaningful results?

To address this question, the scenario can be reconsidered. An electron initially resides in the ground state, and before ionization, its behavior is primarily governed by the Coulomb potential. After ionization, according to the SFA, it is described as a plane wave oscillating in the laser field.

From this perspective, both gauges can be useful. During the first part of the process—when the electron remains bound to the hydrogen atom—the length gauge is more appropriate, as the electron's behavior is better described in terms of its position rather

[1] Higher values of n were tested for lower wavelengths and intensities, but no significant changes in the results were observed.

than its momentum. This is why, in most elementary introductions to light-matter interaction (such as discussions of Rabi oscillations), the length gauge is preferred for systems where ionization does not occur. Conversely, after ionization, the velocity gauge becomes more suitable, as the electron is no longer influenced by the potential (due to the SFA) and is fully characterized by its momentum.

Thus, the length gauge is a fitting choice for the coefficients used in the ODE ansatz.

4.1.2 Full Hilbertspace

The coefficients from the subspace are not the only ones used. A numerical solver (in this case tRecX) was employed to solve the entire TDSE, and the coefficients were extracted from the wavefunction.

As mentioned earlier, there are two ways to consider $\hat{\mathcal{U}}(t', t_0)\,|\Psi\rangle$. First, the TDSE can be solved in the subspace of the bound states (as done with the ODE), or the TDSE can be solved in the full Hilbert space and then projected onto bound states. tRecX implements the second approach, which is significantly more complex than the ODE method. Since far more physical effects influence the time evolution of the coefficients—and consequently the ionization rate—it becomes more challenging to isolate individual effects and their consequences. Nevertheless, having two independent methods that, in some sense, compute the same quantity is useful, allowing for interpretation based on their respective advantages and disadvantages.

For extracting the coefficients from tRecX—i.e., solving the full TDSE and projecting onto bound states—the source code was modified as follows: The occupation probability of specified bound states was already implemented, meaning the code output [2] $\langle\Psi(t)|\hat{P}_{\mathrm{Occ\{H0:n\}}}|\Psi(t)\rangle = |\,\langle\Psi(t)|n\rangle\,|^2$. The main modification involved implementing a new function that replaces the left bra $\langle\Psi(t)|$ with the eigenstate used in $\hat{P}_{\mathrm{Occ\{H0:n\}}}$, while ensuring the eigenstates were normalized. This results in:

$$\langle\Psi(t)|\hat{P}_{\mathrm{Occ\{H0:n\}}}|\Psi(t)\rangle \to \langle n|\hat{P}_{\mathrm{Occ\{H0:n\}}}|\Psi(t)\rangle = \langle n|n\rangle \times \langle n|\Psi(t)\rangle = c_n(t)$$

To achieve this, the eigenvalue problem had to be solved again, and the eigenstates were passed to the function calculating the expectation value. A more elegant and efficient implementation could likely be devised, especially since the eigenstates are already computed elsewhere, but the current approach suffices for now. A detailed description of the changes made to tRecX can be found in [**johannes_porsch_2025_16223179**].

In principle, this is all that is required. However, simply using the coefficients without further scrutiny would be insufficient. Several issues can arise, particularly when extracting

[2] The notation used here follows the same convention as in the code for better reference.

values from code not originally designed for this purpose. This is especially relevant when computing quantities that are not experimentally accessible or are gauge-dependent, as such results would typically be of limited utility. Thus, caution is necessary.

Gauge dependence The coefficients are gauge-dependent, similar to the subspace approach using the ODE. However, in tRecX, a 'hybrid gauge' is employed. This means that within a certain radius R_g from the nucleus, length gauge is used, while outside this radius, velocity gauge is applied. Length gauge is better suited for pre-ionization dynamics, as the electron's behavior is more accurately described by its position rather than its momentum. The gauge radius must be chosen carefully to ensure that pre-ionization dynamics are not computed in velocity gauge. To verify the gauge consistency of the coefficients, they were compared with the ODE approach, which operates strictly in length gauge.

States used in the SFA rate A similar issue arises with the tRecX coefficients as with the ODE coefficients: determining how many should be included in the calculation. Unlike the subspace approach, ionization is permitted here, so including higher bound states is not expected to cause the same numerical difficulties as before. However, the gauge radius should not be exceeded, as beyond this point, the coefficients correspond to the velocity gauge, which may produce incorrect or unphysical results. To minimize numerical issues, only the first few bound states are typically used for the SFA rate. This choice can be justified by examining the populations of the hydrogen atom, where most dynamics occur within the $1s$, $2s$, $2p$, and $3p$ states.

4.2 Dipole Matrix Elements

The dipole transition matrix elements $\mathbf{d}_{nlm}(\mathbf{p})$ from a certain bound state to the continuum states are somewhat less ambiguous than the coefficients. Calculating them in general is difficult, but in the case of hydrogen, an analytical solution is possible. A detailed derivation can be found in Appendix A. The actual calculation of the formula for implementation in the code was performed in a Mathematica notebook, which can be found in the electronic appendix [**johannes_porsch_2025_16223179**].

As mentioned in the theory section, this simplicity in calculation is only possible due to the strong approximation made with the SFA regarding the dipole matrix elements. The final state after ionization is not truly a plane wave but is approximated as such under the SFA.

As discussed in the coefficients section, not all states contribute equally to the ionization dynamics. Besides the ground state $1s$, this thesis restricts calculations to the states $2p$

and $3p$. Most of the pre-ionization dynamics is determined by these states; including additional states would primarily refine the ionization rate rather than introduce significant new physics.

Simplifying the matrix elements is also crucial to avoid numerical instabilities. Particularly when integrating over the azimuthal angle ϕ_p in the final rate, where exact cancellations are expected, limited numerical precision can lead to incorrect results.

The dipole matrix elements can be simplified by noting that the ground state is $1s$ and the light wave is linearly polarized, ensuring that all other states also have $m = 0$. Since the derivation is lengthy, it is provided in Appendix A as well.

4.3 TIPTOE Simulations

As discussed in Chapter 3, TIPTOE is used in this thesis to compare the ionization yield obtained from the SFA rate and the numerical solution of the TDSE with tRecX.

In implementation, both approaches can be treated as a type of "machine", where an arbitrary laser field is input and an ionization probability is output. The laser field in this case consists of two pulses in a `cos8` envelope: a strong "fundamental" pulse and a weaker "signal" pulse shifted in time by τ. In tRecX, two laser pulses can be implemented directly. In the SFA rate implemented in Python, the laser field is constructed as an object of the class `LaserField` from the file `field_functions.py`.

Particularly in the SFA rate, numerical challenges arise because the signal pulse acts only as a small perturbation to the fundamental pulse. Care must be taken to ensure that numerical methods accurately capture this perturbation; otherwise, TIPTOE will fail. This challenge is addressed in Chapter 5.

5. Results and Discussion

The biggest benefit of the extended SFA rate in (2.19) is not only that it incorporates more physical effects than standard SFA, but also that, with certain 'tricks,' the influence of different physical effects on the ionization dynamics can be observed. This is preferable to simply presenting a modified rate that yields better results without understanding *why* it yields better results. Before discussing whether the improvement of the SFA rate was successful, it is first necessary to define what can be learned from this kind of generalization.

The goal is to investigate how the incorporation of excited states and the influence of the laser field on the atom affects the ionization process. Specifically, the focus is on determining whether the Stark shift or the distortion of the ground state has a greater impact on the ionization dynamics. This question is answered in this Chapter.

However, a more significant issue is the previously known considerable discrepancy between the overall ionization yield obtained from SFA simulations and the numerical solution of the TDSE. An extended version of the SFA model could help determine whether this discrepancy arises from simplifications in the dynamics before or after ionization. Unfortunately, a fully satisfactory answer to this question cannot be provided in this thesis, even though the theoretical framework of Chapter 2 allows for such an investigation. This remains a topic for future work. This aspect requires additional investigation in future work.

5.1 Comparison of Ionization Dynamics with TDSE using TIPTOE

Improved Reconstruction of Ionization Dynamics The ionization dynamics predicted by the standard SFA approach [**Theory_NPS**] are first compared with the results from the numerical solution of the TDSE. As shown in 5.1(a), the standard SFA generally provides a good reconstruction of the ionization dynamics, though some features are not captured at all[1]. In particular, the off-cycle ionization dynamics exhibits a phase shift that

[1]Note that (3.2) is fulfilled and $\delta N(\tau)$ is proportional to the signal pulse.

does not match the numerical results.

This discrepancy serves as the starting point and motivation of this thesis. To address this, the extended SFA model described in Chapters 2 and 4 was implemented. As previously mentioned, the coefficients can be determined in two ways: either by solving the TDSE in the subspace of the Hilbert space using the system of ODEs or numerically in the full Hilbert space using a numerical solver (here, tRecX). In 5.1(b), the TIPTOE results from both the subspace and full Hilbert space approaches are shown. Importantly, only the first coefficient and first dipole matrix element are used here. In other words, in (2.19), only the first term is considered, i.e., $n_1 = n_2 = 1$. The same formula was already used for simulating the standard SFA model. The only difference is that in the extended SFA model for one state, the coefficient $c_0(t)$ is included, meaning all the differences between the standard SFA and extended SFA in 5.1(b) are solely due to them.

The results indicate that the extended SFA model using coefficients from the full Hilbert space improves the reconstruction of the off-cycle ionization dynamics. Given that only the ground-state coefficients are used and no excited states are included, this represents a significant improvement. Furthermore, as discussed in more detail in Chapter 4, several approximations were made even with the coefficients from the numerical solver.

Interestingly, the TIPTOE measurement with coefficients from the subspace does not differ significantly from the standard SFA model. This suggests that no physical contribution from the coefficients of the wavefunction confined to the subspace of the bound state is captured by TIPTOE in the ionization dynamics. The consequences of this observation are elaborated in the next paragraph.

Additionally, the extended SFA model still appears to lack some physical contributions. Since 5.1(b) does not account for transitions to excited states, this could explain the remaining discrepancies. Another possible reason is the non-negligible role of the Coulomb potential in the ionization process, where the small phase variations in the ionization yield originate from its influence.

Stark shift or distortion of ground state As mentioned in Chapter 2, when ionization is 'turned off' so the wavefunction remains within the subspace of bound states, two major physical effects are carried by the coefficient $c_0(t)$: the Stark shift and the distortion of the ground-state probability amplitude. By using only the phase of $c_0(t)$, the influence of the Stark shift can be isolated:

$$c_n(t) = |c_n(t)|e^{i\phi_n(t)} \rightarrow c_n(t) = e^{i\phi_n(t)} \tag{5.1}$$

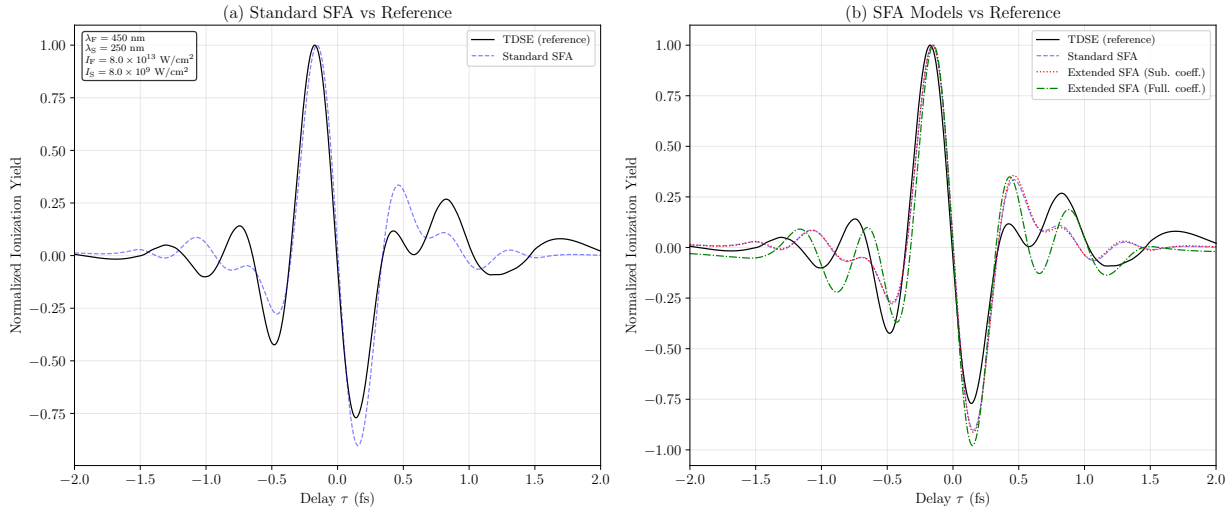

Figure 5.1: Comparison of ionization dynamics predicted between different SFA models and reference data from TDSE using TIPTOE simulations with transitions to excited states neglected. (a) The standard SFA generally provides a reasonable reconstruction of the ionization dynamics, though certain features remain uncaptured. (b) The extended model, with coefficients determined from solving the TDSE in the subspace, exhibits slight improvement. However, when coefficients from the wavefunction restricted to the subspace are used, no significant change or improvement in the dynamics is observed compared to the standard SFA.

However, this approach is valid only for coefficients obtained by solving the TDSE for the wavefunction restricted to bound states, not for the 'Full' approach.

The results using only the phase of the coefficients are shown in figure 5.2(a). Nearly all improvement in ionization dynamics observed with the full Hilbert space coefficients can be attributed to changes in the phase, corresponding to energy level variations over time, while the coefficient amplitudes play a negligible role. As the extended SFA results with coefficients from the subspace showed no improvement, it remains unclear from this plot whether the phase or amplitude dominates.

Initially, it might appear that the improvement in the full Hilbert space TIPTOE result originates from the Stark effect, as suggested by equation (2.20). However, since the Stark effect must be present in both the subspace and full Hilbert space approaches, this provides strong evidence that the Stark effect plays only a minor role in subcycle ionization dynamics. It should be noted that equation (2.20) is valid only for a wavefunction restricted to bound states, which is not the case in the 'Full' approach.

This observation is further supported by the details shown in Figure 5.2(b) and 5.2(c). The phase of the 'Sub' coefficients appears to have a slightly larger impact than their magnitude, though this does not result in any meaningful change in the ionization dynamics

shown in 5.2(a). In contrast, the phase of the coefficients associated with the wavefunction in the full Hilbert space leads to a significant change in the ionization rate, while the distortion in the ground state plays a relatively minor role. When only the magnitudes of the coefficients are compared, the rates are similar, which supports and validates previous arguments.

Additionally, the ionization yield predicted by the extended SFA models in 5.2(b) is slightly lower than that of standard SFA, suggesting that the Stark shift and ground state distortion make ionization 'harder' and less probable for the electron. If this interpretation holds, the electron with the full Hilbert space coefficients should also exhibit reduced ionization when the Stark shift is included. However, 5.2(b) shows the opposite behavior, indicating that the significant change in the rate is attributable to factors other than the Stark shift.

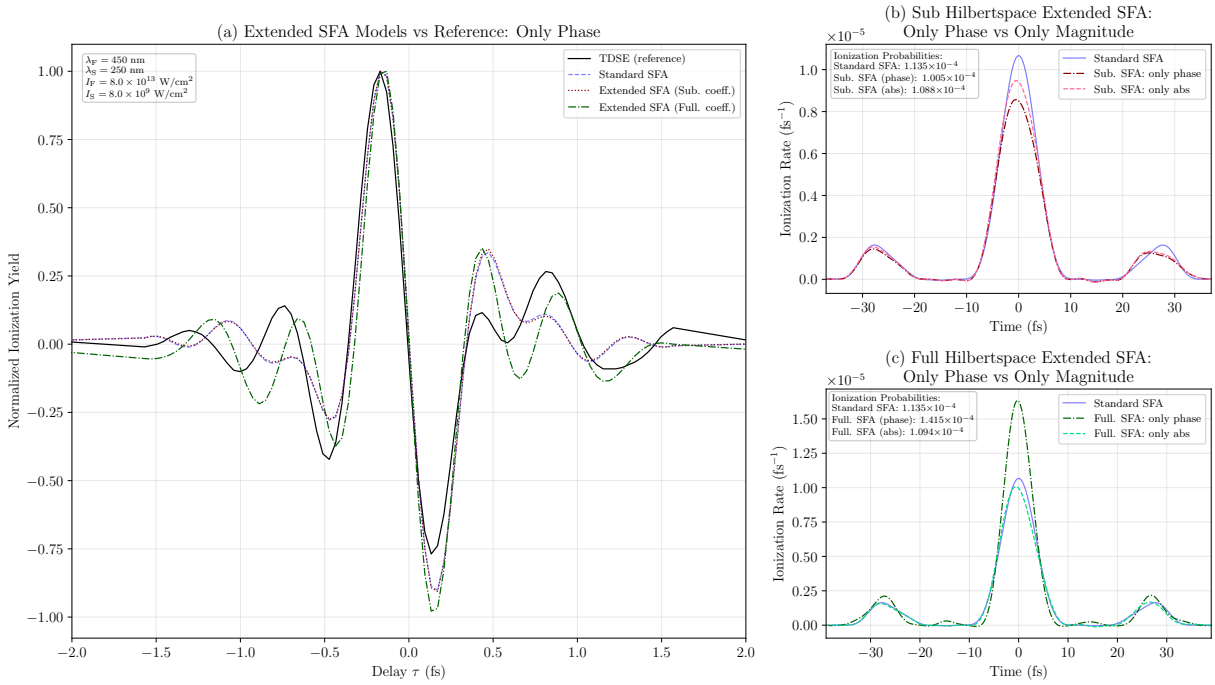

Figure 5.2: Impact of phase and magnitude of the coefficients on TIPTOE simulations and ionization rates for fundamental pulse with transitions to excited states neglected. (a) When only the phase from the coefficients obtained by solving the TDSE in the full Hilbert space is used, an improvement in reconstructing ionization dynamics is observed, while the magnitude of the coefficients appears to have minimal impact. (b) Both the phase and the magnitude of the coefficients are found to have little impact on the ionization rate, though the phase shows slightly more influence. The phase can be interpreted directly as the Stark shift, as suggested by equation (2.20). (c) The magnitude is observed to have a similar influence on the ionization probability as the subspace approach. However, when only the phase of the coefficients from the full Hilbert space is used, a significant difference compared to (b) is observed. This indicates that the change in the ionization rates is not attributable to the Stark effect.

Where does the difference come from? The previous paragraph raises the question of where the improvement between standard SFA and extended SFA with full Hilbert space coefficients originates, if it is not due to the Stark shift or distortion of the ground-state probability amplitude. It should be noted that this is not the focus of the thesis, and thus no definitive answer is provided. However, the difference must arise from effects that manifest in the phase of the coefficients, i.e., in the change of the ground-state energy level over time. Furthermore, this difference is *only* observable when the wavefunction is allowed to ionize, meaning the TDSE is solved in the full Hilbert space. Possible explanations include the influence of the Coulomb potential on ionization dynamics or other effects that are captured by a numerical solver but not by a simple system of ODE's.

5.2 Difference in Ionization Yield between SFA and TDSE

As mentioned in Chapter 3, the ionization yield of the TIPTOE simulations in figures 5.1 and 5.2(a) is normalized to better visualize the actual differences. Further, since the primary focus lies on the dynamics rather than the absolute ionization yield, the normalization is performed according to (3.3). However, in the non-normalized plot, it can be observed that the numerical solution of the TDSE predicts an ionization probability orders of magnitude higher than that of the SFA model. Additionally, small changes in the delay of the signal pulse lead to larger variations in the TDSE results compared to the SFA results, indicating that the 'reference' TIPTOE result is more sensitive to changes in the laser field.

The first observation can be attributed to the fact that in the SFA model, it is assumed that the electron occupies a continuum state after ionization, meaning it no longer experiences the Coulomb potential. This is, of course, a strong assumption and significantly more 'difficult' for the electron to achieve. For this approximation to hold, the laser must effectively 'catapult' the electron out of the atom. Consequently, the overall ionization yield predicted by the SFA model is much lower than that of the TDSE. Second, the numerical solution of the TDSE captures a broader range of dynamics and physical effects during the ionization process. Various processes can occur during this time, which may explain why the ionization yield in the TDSE is more sensitive to changes in the electric field.

While these observations are interesting, they align with the theoretical foundations of the SFA model. To confirm that the discrepancies arise solely from the core assumptions of the SFA model (i.e., the treatment of the final state as a continuum state), other possible explanations must be ruled out. The extended SFA model proposed in this thesis may provide insights into this question. During this research, significant effort has been dedicated to implementing the extended SFA model, particularly to incorporate excited states.

However, due to time constraints, conclusive results on this matter could not be obtained.

Preliminary TIPTOE results suggest that including excited states in the SFA rate partially reduces the order-of-magnitude discrepancy between the SFA and TDSE predictions. Additionally, the cross-coupling terms in (2.19) (i.e., $n_1 \neq n_2$) appear to contribute significantly to the ionization rate. Furthermore, the previously discussed importance of the energy shift in the phase also applies to excited states. The energy level shifts of excited states have a more pronounced effect on the ionization rate than changes in the probability amplitudes of the coefficients. The observed changes in the ionization yield magnitude, potentially arising from the inclusion of excited states in the extended SFA model, may primarily stem from the dipole transition matrix elements. For instance, this could be explained by the laser pulse first exciting the electron to, say, the $3p$ state before ionizing it, leading to a higher overall ionization probability due to additional pathways. However, this hypothesis could not be fully verified here. These indications remain speculative and should not yet be considered definitive results.

6. Conclusion and Outlook

Lorem ipsum dolor sit amet, consetetur sadipscing elitr, sed diam nonumy eirmod tempor invidunt ut labore et dolore magna aliquyam erat, sed diam voluptua. At vero eos et accusam et justo duo dolores et ea rebum. Stet clita kasd gubergren, no sea takimata sanctus est Lorem ipsum dolor sit amet. Lorem ipsum dolor sit amet, consetetur sadipscing elitr, sed diam nonumy eirmod tempor invidunt ut labore et dolore magna aliquyam erat, sed diam voluptua. At vero eos et accusam et justo duo dolores et ea rebum. Stet clita kasd gubergren, no sea takimata sanctus est Lorem ipsum dolor sit amet.

A. Dipole Transition Matrix Elements

Here, the general transition dipole matrix elements into the continuum for a hydrogen atom are derived. The general matrix element in this case is given by:

$$\mathbf{d}_{nlm}(\underline{p}) \overset{\text{a.u.}}{=} -\langle \mathbf{p}|\hat{\mathbf{r}}|\Psi_{nlm}\rangle$$

where $|\mathbf{p}\rangle$ is a plane wave. The wave function for the hydrogen atom is well known:

$$\Psi_{nlm}(\underline{x}) = \langle \mathbf{r}|\Psi_{nlm}\rangle = R_{nl}(r)Y_{lm}(\theta_r, \phi_r) \tag{A.1}$$

with $R_{nl}(r)$ being the radial part of the wavefunction and $Y_{lm}(\theta_r, \phi_r)$ being the spherical harmonics.

By partitioning the $\hat{1}$ operator and using the fact that $\underline{\mathbf{r}} \to i\nabla_{\underline{p}}$ in momentum representation, a general formula for the transition is obtained:

$$\mathbf{d}_{nlm}(\underline{p}) = -i\nabla_{\underline{p}} \int \mathrm{d}^3\underline{x}\, \psi_{nlm}(\underline{x}) e^{-i\mathbf{p}\cdot\mathbf{r}} = -i\nabla_{\underline{p}}\phi_{nlm}(\underline{p})$$

In principle, this integral (i.e the Fourier transform) is all that is required. Due to the structure of ψ_{nlm}, a result similar to (A.1) can be expected. A posteriori, it can be shown that:

$$\mathcal{F}\{\psi_{nlm}(\underline{x})\} = \phi_{nlm}(\underline{p}) = F_{nl}(p)Y_{lm}(\theta_p, \phi_p)$$

where $F_{nl}(p)$ is the Fourier transform of the radial part of the wavefunction and $Y_{lm}(\theta_p, \phi_p)$ are the spherical harmonics in momentum space, analogous to the hydrogen atom in position space.

Momentum space

The so-called plane wave expansion [**Jackson:1998nia**] of the exponential part of the integral is given by:

$$e^{i\mathbf{p}\cdot\mathbf{r}} = \sum_{l'=0}^{\infty}(2l'+1)i^{l'}j_{l'}(pr)P_{l'}(\mathbf{p}\cdot\mathbf{r}) = 4\pi\sum_{l'=0}^{\infty}\sum_{m'=-l'}^{l'} i^{l'}j_{l'}(pr)Y_{l'm'}(\theta_p, \phi_p)Y^*_{l'm'}(\theta_r, \phi_r)$$

Here, $j_l(pr)$ represents the spherical Bessel functions, and the integration is performed over spherical coordinates. While the expression initially appears complex, the orthogonality of the spherical harmonics can be used to simplify the integral to:

$$\phi_{nlm}(\underline{p}) = 4\pi \sum_{m=-l}^{l} Y_{lm}(\theta_p, \phi_p) i^l \underbrace{\int_0^\infty \mathrm{d}r\, r^2 j_l(pr) R_{nl}(r)}_{\tilde{R}_{nl}(p)}$$

This structure is the desired form. The focus now shifts to the radial part $\tilde{R}_{nl}(p)$ of the integral. The term $R_{nl}(r)$ corresponds to the radial function of the hydrogen atom in position space and is independent of the magnetic quantum number m. It consists of an exponential term dependent on r, a polynomial term dependent on r, the generalized Laguerre polynomials, and the normalization constant. A closed expression for the generalized Laguerre polynomials would be convenient. They are represented as:

$$L_n^l(r) = \sum_{\iota=0}^{n} \frac{(-1)^\iota}{\iota!} \binom{n+l}{n-\iota} r^\iota$$

Thus, the Laguerre polynomials depend only on an exponential term and finitely many polynomial terms. $\tilde{R}_{nl}(p)$ can be expressed (without prefactors and summation over ι) as:

$$\int_0^\infty \mathrm{d}r\, r^{2+l+\iota} e^{-\frac{Zr}{n}} j_l(pr)$$

Before solving the integral using computational methods, the spherical Bessel function must be transformed into ordinary Bessel functions:

$$j_l(pr) = \sqrt{\frac{\pi}{2pr}} J_{l+\frac{1}{2}}(pr)$$

At this stage, it is useful to combine all prefactors and summations into a single expression and examine the integral as a whole:

$$\begin{aligned}\phi_{nlm}(\underline{p}) = {} & \frac{\pi^{3/2}}{\sqrt{2p}} \sqrt{\left(\frac{2}{n}\right)^3 \frac{(n-l-1)!}{n(n+1)!}} \\ & \times \sum_{m=-l}^{l} \sum_{\iota=0}^{n-l-1} i^l \frac{(-1)^\iota}{\iota!} \left(\frac{2}{n}\right)^{l+\iota} \binom{n+l}{n-l-1} \underbrace{\int_0^\infty \mathrm{d}r\, r^{l+\iota+\frac{3}{2}} e^{-\frac{Zr}{n}} J_{l+\frac{1}{2}}(pr)}_{(*)} Y_{lm}(\theta_p, \phi_p)\end{aligned} \tag{A.2}$$

The remaining integral was computed using Mathematica, so a detailed derivation is not provided. Interestingly, an analytical solution exists. The result for $(*)$ is:

$$(*) = {}_2\tilde{F}_1\left(2 + l + \frac{\iota}{2}, \frac{1}{2}(5 + 2l + \iota); \frac{3}{2} + l; -\frac{n^2p^2}{Z^2}\right)$$

Here, ${}_2\tilde{F}_1$ denotes the regularized hypergeometric function, defined as:

$${}_2\tilde{F}_1(a, b; c; z) = \frac{{}_2F_1(a, b; c; z)}{\Gamma(c)} = \frac{1}{\Gamma(a)\,\Gamma(b)} \sum_{n=0}^{\infty} \frac{\Gamma(a+n)\,\Gamma(b+n)}{\Gamma(c+n)} \frac{z^n}{n!}$$

The final expression for $\phi_{nlm}(\underline{p})$, which can also be found in [**Bransdenatomsmolecules**] in a slightly different form, is given by:

$$\begin{aligned}\phi_{nlm}(\underline{p}) = \sum_{\iota=0}^{2l+1} & \frac{(-1)^\iota\, 2^{\iota+\frac{1}{2}}\, n\, (in)^l\, (p^2)^{l/2}\, Z^{-l-3}\, \Gamma(2l+\iota+3)}{\iota!} \\ & \times \binom{l+n}{-l+n-\iota-1} \sqrt{\frac{Z^3\Gamma(n-l)}{\Gamma(l+n+1)}} \\ & \times Y_l^m(\theta_p, \phi_p)\, {}_2\tilde{F}_1\left(l + \frac{\iota}{2} + 2, \frac{1}{2}(2l+\iota+3); l + \frac{3}{2}; -\frac{n^2p^2}{Z^2}\right) \end{aligned} \tag{A.3}$$

Improved rate

Usually all that remains is to differentiate (A.3) with respect to $\underline{p}$. However, before that, the SFA rate can be improved directly by performing the integration over ϕ_p analytically. The rate according to Chapter 2 is given by:

$$\begin{aligned}\Gamma_{\mathrm{SFA}}(t) = \sum_{n_1} \sum_{n_2} & \int_0^\infty \mathrm{d}p\, p^2 \int_0^\pi \mathrm{d}\theta_p\, \sin\theta_p \int_0^{2\pi} \mathrm{d}\phi_p \int_{-\infty}^{\infty} \mathrm{d}T \\ & \times \exp\left(i\mathbf{p}^2 T + ip\cos\theta_p \bar{\Delta}_z^k + \frac{i}{2}\bar{\Delta}_z^2 + i(t-T)E_{n_1} - i(t+T)E_{n_2}\right) \\ & \times E_z(t-T)E_z(t+T)c_{n_1}^*(t-T)c_{n_2}(t+T)d_{z,n_1}^*(\underline{p} + \Delta_z(-T))d_{z,n_2}(\underline{p} + \Delta_z(T))\end{aligned}$$

As mentioned before, the dipole transition matrix element can be written in the following convenient form:

$$d_{z,nlm}(\underline{p}) = \left[-i\nabla_{\underline{p}}\phi_{nlm}(\underline{p})\right]_z = -iY_{lm}(\theta_p, \phi_p)\left(\cos\theta_p \frac{\partial F_{nl}}{\partial p} - \frac{\sin\theta_p}{p}\frac{\partial F_{nl}}{\partial p}\right)$$

Note that here the z component of a gradient in spherical coordinates was taken. The exact formula can be easily computed using the transformation between Cartesian and spherical coordinates.

The integration over θ_p is difficult and might not be possible to perform analytically. However, for the integral over ϕ_p, only the following needs to be solved:

$$\begin{aligned}\int_0^{2\pi} \mathrm{d}\phi_p \, Y^*_{l'm'}(\theta_p, \phi_p) Y_{lm}(\theta_p, \phi_p) &= \frac{1}{4\pi} \sqrt{(2l+1)(2l'+1)\frac{(l-m)!(l'-m')}{(l+m)!(l'+m')!}} \int_0^{2\pi} \mathrm{d}\phi_p \, \mathrm{e}^{i(m-m')\phi_p} \\ &= \frac{1}{2} \sqrt{(2l+1)(2l'+1)\frac{(l-m)!(l'-m)}{(l+m)!(l'+m)!}}\end{aligned}$$

This means that the magnetic quantum number is conserved during the transition between two arbitrary states. Since the initial state is the ground state $1s$, m is zero here and therefore everywhere. This significantly simplifies the expression.

Declaration on the Use of AI Tools

During the preparation of this thesis, artificial intelligence (AI) tools were used. Specifically, ChatGPT, DeepSeek, Gemini 2.5 Pro, and GitHub Copilot were employed for proofreading and grammar correction of the text, as well as for formatting Python code used in generating plots and processing data. Additionally, AI-assisted methods were applied to identify relevant academic papers during the literature search.

Eigenständigkeitserklärung

Hiermit erkläre ich, die vorliegende Arbeit selbständig verfasst zu haben und keine anderen als die in der Arbeit angegebenen Quellen und Hilfsmittel benutzt zu haben.

München, den 22. Juli 2025

_____

Unterschrift